European Polymer Journal 46 (2010) 2206–2215

Contents lists available at ScienceDirect

European Polymer Journal

journal homepage: www.elsevier.com/locate/europolj

Effect of highly filled ferrites on non-isothermal crystallization behavior of polyamide 6 bonded ferrites

Caiyun Jiang, Dapeng Wang *, Maojie Zhang, Peijun Li, Shugao Zhao **

Key Laboratory of Rubber-Plastics, Ministry of Education, Qingdao University of Science and Technology, Qingdao 266042, People's Republic of China

ARTICLE INFO

Article history:
Received 17 December 2009
Received in revised form 7 April 2010
Accepted 2 May 2010
Available online 8 May 2010

Keywords:
Polymer bonded magnets
Non-isothermal crystallization
Highly filled systems
Polyamide 6

ABSTRACT

The aim of this study is to characterize the non-isothermal crystallization of polyamide 6 bonded highly filled ferrites which were prepared by the melt extrusion. Especially, the effect of ferrite concentration and its surface property on the non-isothermal crystallization were investigated by means of differential scanning calorimetry. The highly filled ferrite particles acting as obstacles could severely hinder the motion of surrounding chain segments, which were irrespective of surface nature. The ferrite could be modified by silane and obtain a visually enhanced interaction with polymer matrix which evoked the heterogeneous nucleation. Increasing this enhanced interfacial area between polymer–particle can promote the heterogeneous nucleation. However, a strong interaction can slow the motion of surrounding chain segments of particles, thereby producing a competitive effect on the crystallization rate and crystallinity. The plot of crystallization activation energy against concentration also can evaluate dispersion performance of hydrophilic fillers within hydrophobic polymer.

1. Introduction

Polymer bonded magnets (PBMs) as one of the more important developments in magnetic materials in recent years, have opened a new world of application opportunities. PBMs composed of polymeric matrices and magnetic fillers (e.g. ferrites, NdFeB, SmCo) can be produced by conventional polymer processing methods, and offer significant advantages, in terms of processing and cost, as compared with their metallic counterparts [1–20]. However, the introduction of a small quantity of semicrystalline engineering plastics as binders dilutes the concentration of magnetic powders, resulting in low magnetic performance. Moreover, the applications of PBMs were limited because highly filled magnetic fillers can severely increase the apparent viscosity of polymer flow and further make the processing difficult. In addition, highly filled fillers not only evoked damage of polymer continuous matrix, but also impacted the crystallization behavior of semicrystalline polymer, (e.g. polyamide, poly(*p*-phenylene sulfide), etc.), suggesting a macroscopic influence of mechanical properties. Furthermore, the crystallization behaviors of semicrystalline polymer composites as a function of processing conditions are of great importance in polymer processing, particularly for the analysis and design of processing operations [21]. Hence, it is important to understand the effect of highly filled particles on the crystallization of semicrystalline polymer matrix.

So far, there were only a minority of existing works focusing on the crystallization of the highly filled fillers/semicrystalline polymer systems. Otaigbe et al. [11] investigated isothermal crystallization of PPS/NdFeB composites and disclosed that NdFeB particles modified by silane acted as the nucleation agent and accelerated the crystallization of polymer. Furthermore, particle size distribution did not affect the crystallinity of the composite significantly. On the contrary, according to Khalil and co-author's report [22], the highly filled rice hull ash within polypropylene

* Corresponding author.
** Corresponding author. Tel.: +86 532 84022936; fax: +86 532 84882744.
E-mail addresses: amandajiang1120@hotmail.com (C. Jiang), wangd@mpip-mainz.mpg.de (D. Wang), zhangmj@iccas.ac.cn (M. Zhang), li@qust.edu.cn (P. Li), zhaosgqd@hotmail.com (S. Zhao).

0014-3057/$ - see front matter © 2010 Elsevier Ltd. All rights reserved.
doi:10.1016/j.eurpolymj.2010.05.002

matrix did not play a role as the nucleation agent but hindered the crystallization, due to the fact that highly filled particles confined the motion of polymer chain. However, for highly filled organically modified montmorillonite (MMT)/maleic anhydride grafted polyethylene nanocomposites, the MMT had no significant effect on the total non-isothermal crystallization due to neutralizing effect [23]. There were also some studies on the crystallization of highly filled systems such as PMMA-layered silicate nanocomposites [23,24], organic matter/PP composites [25], Chlorinated polyethylene/layered silicate nanocomposites [26], etc. In spite of the extensive theoretical and experimental effect in the past decade, the effect of highly filled fillers on the crystallization of semicrystalline matrix is still unclear. The role of highly filled fillers within polymer matrix upon crystallization process still remains an open question.

In this paper, a method of non-isothermal crystallization which is closely related to manufacture process was adopted to study the crystallization behavior of polyamide 6 (PA6) bonded highly filled ferrites. For magnetic material, ferrites have inferior magnetic performance and be geared to the needs of low-end fields. The ferrites as inorganic particles can be modified by silane [11,27] and titanate [28]. On the other hand, PA6 is a typical polyamide with several attractive advantages such as high strength, good toughness and abrasion resistance, which is regarded as the appropriate polymeric matrices for PBMs. The ferrites/PA6 composites are considered as model systems to explore the intrinsic non-isothermal crystallization behavior and kinetic of highly filled systems. The non-isothermal melting process together with cooling process was involved to study the substantive characteristics of the interaction between polymer and particles.

2. Experimental

2.1. Materials

Polyamide 6 powder used were obtained commercially from Nanjing Hongrui Plastic Products Co., Ltd. (China). The density, melting point, heat distortion temperature and molecular weight of PA6 were 1.13 g/cm^2, 216 °C, 201 °C and 27,500, respectively. The magnetic powder: ferrites with density of 5.1 g/cm^2 and hydrophilic surface, manufactured by BGRIMM Magnetic Materials & Technology Co., Ltd. (China), consisted of a $6Fe_2O_3{\cdot}SrO$ alloy ($SrFe_{12}O_{19}$) with various particle sizes being produced in block form (see inset of Fig. 1). The particle size distribution utilized ranged from 0.1 to 4 μm is determined by randomly measuring 100 ferrite particle from the inset of Fig. 1, as shown in Fig. 1. *N*-(2-aminoethyl)-3-aminopropyltrimethoxysilane (CAS: 1760-24-3) produced by Nanjing Xiangfei Chemical Research Institute (China) was utilized as the coupling agent.

2.2. Sample preparation

The polymers and magnetic fillers were dried at 80 °C in a vacuum oven for 24 h before use. Before melt extrusion, quantitative PA6, ferrites and silane (1 wt% of ferrites, if there was) were mixed under strenuous stirring, and then the mixture was extruded with a Brabender two-screw extruder (ZKS-25, Krupp Werner & Pfleiderer GmbH, Stuttgart, Germany). The temperature of the extruder was maintained at 190, 220, 230, 240 and 250 °C from hopper to die, respectively. The rotation speed of the twin screw was 80 rpm. The neat PA6 was also extruded under the same condition. In the paper afterward the PA6 bonded ferrites with rough ferrite volume concentration of *j*% was referred to as PA6-j and the subscribed 'S' was added for silane modified sample. For example, PA6-46 used for PA6/ferrites with volume ratio of 54/46, $PA6_S$-46 used for PA6/ferrite/silane with volume ratio of 51.76/46/2.23, calculated based on their density.

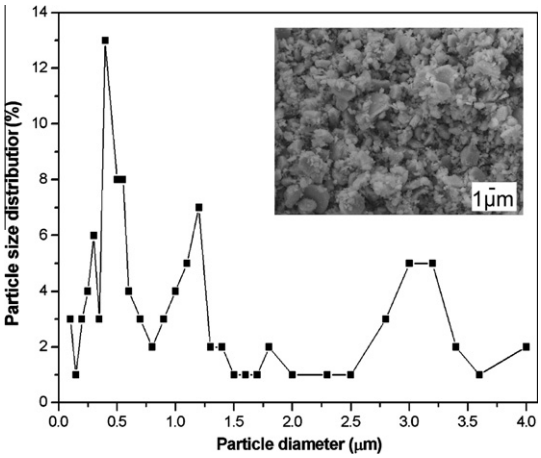

Fig. 1. The particle size distribution of ferrites is determined by randomly measuring 100 ferrite particles from the inset SEM photograph of ferrites.

2.3. Scanning electron microscope (SEM)

The morphologies of ferrites and PA6/ferrite composites were examined with a JEOL JSM-6700F for SEM experiment. The specimens were fractured by tensile testing with the drawing speed of 10 cm/s. The tensile fracture surfaces were coated with a thin layer of gold by JFC-1600 Auto Fine Coater and then examined by SEM.

2.4. Differential scanning calorimetry (DSC)

PerkinElmer DSC-7 calorimeter was used to characterize the cooling and melting process. The samples were dried under vacuum at 80 °C for 24 h to remove any remaining water. About 5 mg of the polymer samples was weighed accurately in the aluminum pan and placed in the DSC cell. All DSC analyses were performed under nitrogen atmosphere. The non-isothermal crystallization of PA6 and its composites were performed as follows: the sample was heated from 20 to 245 °C, at a heating rate of 40 °C/min. The sample was kept for 10 min at 245 °C to eliminate the thermal history. Then the sample was cooled to 100 °C at a heating rate of 40 °C/min. The non-isothermal crystallization behaviors were investigated by cooling samples from 245 to 100 °C at a constant cooling rate of

2.5, 5, 10, 20 °C/min, respectively. The thermograms were recorded to estimate the non-isothermal crystallization kinetics. The sample was heated from 100 to 245 °C, at a heating rate of 20 °C/min to record the melting behavior.

3. Results and discussion

3.1. Morphologies by SEM

The SEM micrographs considered as the most intuitive method, could exhibit the morphologies of surface fractures of PBMs. Fig. 2 displays different interfacial properties of modified and rough ferrites within PA6 matrix with the same ferrite concentration. The debonding pointed-out by a black arrow in Fig. 2(b) reflects the visual incompatibility between rough ferrites and PA6, resulting in a distortion and further, damage of polymer continuous matrix. The highly filled ferrites, therefore, might hinder the motion of polymer segments. In addition, both the incompatibility and particle agglomeration could give rise to some space within the matrix. On the contrary, the interface between PA6 and silane modified ferrites with partial hydrophobic surface is blurry and has no obvious cavities within the whole field of view, except for some particles over a size scale less than rough 200 nm (see inside of black circle in Fig. 2(d)). We attribute this to the incomplete modification. Note that it is difficult to observe the dispersion (homogeneous or agglomeration) of highly filled particles in PA6 matrix. However, we believe highly filled ferrites always form agglomeration which is independence of surface property, shape and size. The particles are too crowding to have enough space to form good dispersion.

The modified ferrites are seen to have a relatively good interaction with PA6, stemmed from hydrogen bonding between amino group of silane on the surface of ferrites and carbonyl group of PA6, as proved by FTIR measurement (Fig. 3).

For pure PA6, the strong band attributed to hydrogen bonded N–H stretching vibration with C=O can be observed at 3296.2 cm^{-1}, the absorption peak at 3085 cm^{-1} indicate the hydrogen bonds of COOH [29]. The absorption band at 1633.6 and 1539.0 cm^{-1} is due to C=O stretching vibration of amide I band and N–H deformation vibration of the amide II band, respectively [30,31]. The facts that the absorption bands at 3296.2 and 1539.1 cm^{-1} shift to low wavenumber direction and the band at 3085 cm^{-1} nearly disappear jointly indicate highly filled ferrites irrespective surface property weaken of the hydrogen bond within PA6 matrix [32]. The amide I region is composed of maximum three bands attributable to hydrogen bonded carbonyl group in ordered domains (corresponding to band at 1636 cm^{-1}), hydrogen bonded carbonyl group in disorder conformations (corresponding to band at 1645 cm^{-1}), and "free" carbonyl groups (corresponding to band at 1680 cm^{-1}) [33,34]. It is expected to see that the amide I region of PA6, move to higher frequency, as incorporation of ferrites, indicating that the forming of disordered hydrogen bonding between C=O in PA6 and N–H in silane for the $PA6_S$-46. The introduction of unmodified ferrites also can shift the amide I region to high frequency direction, resulted from the hydrogen bonding between C=O in the PA6 chain and O–H of residual water on rough ferrite surface, which is distinctly weaker than that on modified ferrite surface. We also observe that for $PA6_S$-46, a relatively strong hydrogen bonding in ordered domains, which corre-

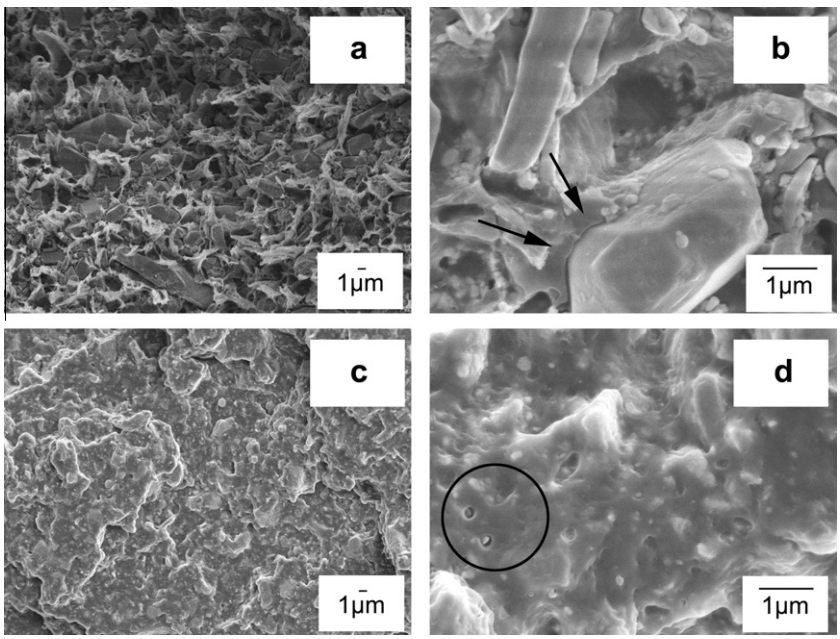

Fig. 2. SEM photographs of fracture surfaces of (a and b) PA6-46 and (c and d) $PA6_S$-46 with the magnification for (a and c) 3000× and (b and d) 20,000×.

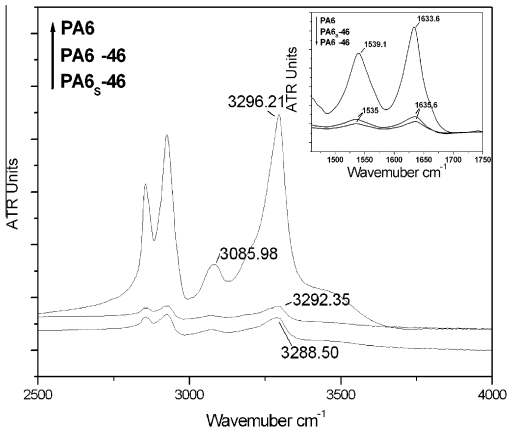

Fig. 3. FTIR spectrums of pure PA6 and PBMs.

sponds to a higher crystallinity, as compared to the FTIR data of PA6-46.

SEM images presented are obtained from the fractured surfaces after the tensile tests. Therefore, the stress and strain applied on the sample might have distorted the original morphology of the composites. Thus, to obtain a deeply insight into interaction and its effect on the crystallization, the non-isothermal behaviors will be involved in the next section.

3.2. Non-isothermal crystallization and subsequent melting behavior

From a practical industrial point of view, it is important to characterize the non-isothermal heating and cooling process of polymeric materials, because the polymer is performed under non-isothermal conditions during fabrication. The non-isothermal curves of PA6 and PA6 bonded ferrites are normalized by polymer weight percentage, as shown in Fig. 4. From these curves, some useful parameters, such as crystallization initiating (T_i), peak (T_p) and finishing (T_f) temperature, crystallization activation energy (ΔH_c) and the viscous flow activation energy (ΔH_m) are obtained and tabulated in Table 1, which reveal some pertinent differences:

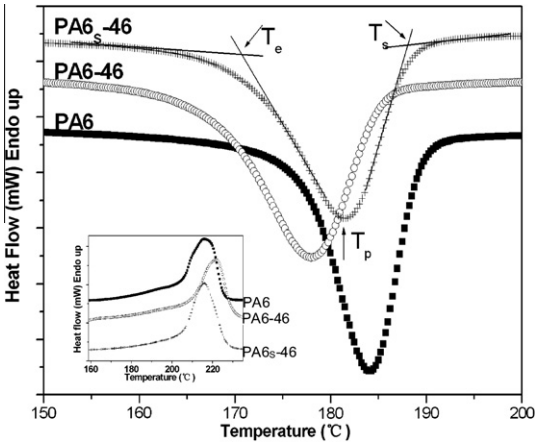

Fig. 4. Non-isothermal crystallization and melting (inset) behaviors of PA6, PA6-46 and PA6$_S$-46 with cooling and heating rates of 20 °C/min.

(a) The crystallization peak volume of PA6-46 sample becomes broader and weaker, and shifts to lower temperature, as compared with that of PA6. This is ascribed to the fact that highly filled ferrites act as obstacles and hinder the motion of surrounding chain segments, which is in agreement with our SEM image predictions and the results of previous works [23,35–38]. This hindering effect is aggravated as increasing the rough ferrite concentration [39,40]. In addition, the increase of melting point of PA6-46 is considered as next direct evidence for the confined motion of chains. However, the particle agglomeration introduces some space within polymer matrix to promote the mobility of segments and thus is responsible for a decreased T_f.

(b) A less supercooling ($\Delta T = T_m - T_p$) of polymer composites reflects a heterogeneous nucleation mechanism [21]. In this case, silane modified ferrite particles with a incomplete hydrophobic surface acting as the nucleation agent initiate the heterogeneous nuclei as soon as the specimens reach the crystallization temperature [39], as displayed in Table 2. The PA6$_S$-0.5 obtains the smallest supercooling indicate the occurrence of heterogeneous nucleation mechanism while only 0.5 vol % ferrites escape the possibility of the hindering effect. The good interaction observes in Fig. 2(c) and (d) is responsible for this heterogeneous nucleation. Compared with the supercooling data of PA6$_S$-46 and PA6$_S$-60, it is seen that increasing the enhanced interfacial area could promote the heterogeneous nucleation. The crystal form of polymer is more perfectly with smaller supercooling than that with larger supercooling. We envisage that the effect of concentration variation of highly filled particles on the distortion and damage of polymer matrix is negligible and thus, a higher crystallinity for the sample with more hydrophobic ferrite surface is observed. Hence, both the interfacial area and strength between polymer and particles is the key for particle to be the nucleation agent.

The crystallization study of PA6 should be in a very confined condition. Since the modification of ferrites decrease the density and thus, the volume percent of PA6 in PA6$_S$-46 is practically lower than that in PA6-46. However, if we keep the volume percent of PA6 constant, it is equal to reduce the particle concentration within PA6 matrix. In other word, the degree of crowd of particles in PA6 matrix decrease. Fortunately, for the highly filled systems, the slight variation of particle concentration scarcely change the polymer based property, namely, the crystallization, rheology and mechanical properties. However, the magnetic property is highly sensitive to the mass percent of rough ferrites at highly loaded level. In order to confirm the discussion above, we also prepared another sample (PA6$_S$-43.8) which obtains the same volume percentage of PA6 as compared to PA6-46. The change of crystallization behavior is quite small. Thus, in this study, we ignore the slight variation of volume percent of PA6 between PA6-46 and PA6$_S$-46.

(c) Compared with the crystallization peak of PA6-46 and PA6$_S$-46 at low temperature regime (160–175 °C), it

Table 1
DSC data for PA6 and PA6 bonded ferrites, obtained from the cooling and heating DSC curves.

Sample	$T_{m,peak}$ (°C)[a]	ΔH_m (J/g)[a,e]	T_i (°C)[b]	T_p (°C)[b]	T_f (°C)[b]	ΔH_c (J/g)[b,e]	ΔT (°C)[c]	X_c (%)[d]
PA6	216.0	57.2	189.6	184.3	177.0	58.4	32.0	23.8
$PA6_S$-0.5	217.3	58.0	191.7	186.9	179.4	59.1	29.6	24.1
PA6-5	221.5	57.6	188.9	183.3	174.7	68.1	38.2	24.0
PA6-20	220.5	52.1	187.7	181.8	172.2	57.0	38.7	21.7
PA6-46	221.5	41.5	185.7	178.1	167.5	57.5	43.4	17.2
$PA6_S$-46	215.5	47.7	188.2	181.6	170.8	61.6	33.9	19.9
$PA6_S$-60	215.0	52.1	189.7	182.6	170.1	58.0	32.4	21.7

[a] T_m and ΔH_m measured on the second heating at 20 °C/min.
[b] T_i, T_p, T_f and ΔH_c measured on the first cooling at 20 °C/min.
[c] Degree of supercooling, $\Delta T = T_m - T_p$.
[d] Crystallinity of degree, $X_c = \Delta H_m/\Delta H_m^\circ$ (ΔH_m° = 240 J/g is the heat fusion of PA6 [45]).
[e] ΔH_m and ΔH_c are normalized by polymer weight percentage.

Table 2
Non-isothermal crystallization kinetic parameters based on the Avrami method.

Cooling rate (°C/min)	2.5	5	10	20
PA6				
n	6.2	7.3	7.7	7.6
Z_c (min^{-n})	2.2E−02	1.8E−01	5.4E−01	9.1E−01
PA6-5				
n	6.6	9.5	12.7	9.7
Z_c (min^{-n})	3.3E−02	1.8E−01	4.8E−01	9.0E−01
PA6-20				
n	7.2	10.1	11.1	10.8
Z_c (min^{-n})	2.8E−02	1.4E−01	5.3E−01	8.9E−01
PA6-46				
n	7.7	9.7	11.6	12.9
Z_c (min^{-n})	3.7E−03	1.4E−01	5.0E−01	7.9E−01
$PA6_S$-46				
n	6.9	7.5	8.7	9.2
Z_c (min^{-n})	1.9E−02	2.0E−01	5.6E−01	9.4E−01
$PA6_S$-60				
n	6.5	7.1	8.3	9.1
Z_c (min^{-n})	2.5E−02	2.2E−01	5.5E−01	8.9E−01

is observed that the shape of both curves are quite similar and both broader than that of PA6. We attribute this to the hindering effect of particles upon crystallization process being independence of surface nature within PA6. The finishing temperature of $PA6_S$-46 is higher than that of PA6-46, because the enhanced interfacial strength "absorbs" the surrounding chain segments and reduces mobility of chain segments.

(d) Note that, the PBMs sample with a small quantity of ferrites (i.e. 5 vol %) obtains an increase of crystallinity. The result is consistent with the crystallization behavior of a lot of polymer nanocomposites [21,41–43] whereas on the basis of a different mechanism. Some spaces on the interface promote the mobility of chain segments even at a relatively low temperature. The supercooling data and decreased T_f of PA6-5 jointly indicate that an enhanced mobility of segment (capability of crystallization in low temperature) instead of heterogeneous nucleation gives rise to the increase of crystallinity for PA6-5.

Several previous works verified that low or high content of nanoscale particles in polymer matrix can evoke a heterogeneous nucleation [21,23,36,37,40–45]. For particles with wide size distribution and above a size scale of nano-level, however, heterogeneous nucleation mainly depends on the interfacial area and strength. Thus, it is reasonable to interpret that the modified NdFeB with hydrophobic surface had strong interaction with hydrophobic PPS and hence acted as the nucleation agent [11]. The rice hull ash with hydrophobic surface was "soft" and did not form a strong interaction with polypropylene, which just retarded the crystallization [22].

Some fillers will promote the formation of γ-crystal of PA6, for example clay, but other fillers can favor the formation of α-crystal of PA6, for example carbon nanotube, carbon fiber, etc. Based on existing study [46], the influence of low loaded ferrites on the crystalline morphology is little. However, the XRD is currently un-accessible for the highly filled samples due to the big noise probably generated by highly filled ferrites.

3.3. Non-isothermal crystallization kinetics

According to the DSC thermograms of non-isothermal crystallization scans, the values of the relative crystallinity at different cooling rates can be determined by the following equation [47]:

$$X_t(t) = \frac{\int_{t_0}^{t}(dH_c/dt)dt}{\int_{t_0}^{t_\infty}(dH_c/dt)dt} = \frac{A_0}{A_\infty}, \quad (1)$$

where the dH_c/dt is the rate of heat evolution, t_0 and t_∞ are the temperatures, at which the crystallization starts and ends, A_0 and A_∞ are areas under the normalized DSC curves. The crystallization time (t), can be transformed from the corresponding temperature T by means of the following equation:

$$t = \frac{|T_0 - T|}{a}, \quad (2)$$

where T_0 is the initial temperature of crystallization behavior and a is the cooling rate. In this paper, PA6 and $PA6_S$-46 are selected as model samples to plot the curves of non-isothermal crystallization kinetic. The non-isothermal crystallization exothermic peak of PA6 and $PA6_S$-46 at various cooling rate a, are shown in Fig. 5. It is well known that the increase of cooling rate can broaden the crystallization peak and shift it to low temperature direction, vice versa. From the DSC digital information, the relative crys-

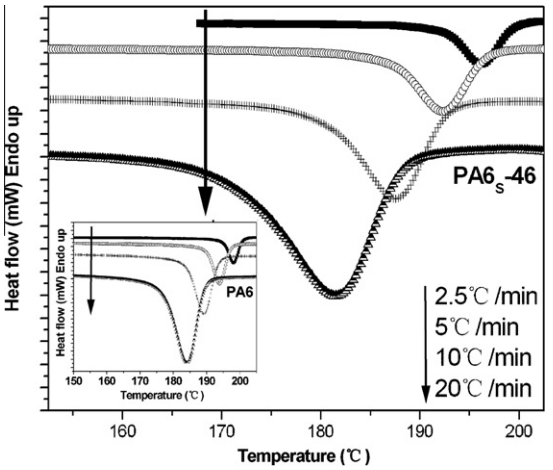

Fig. 5. Non-isothermal crystallization curves of PA6$_S$-46 and PA6 (inset).

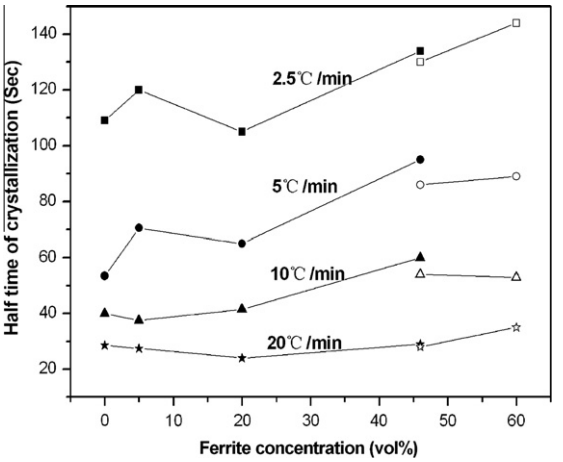

Fig. 7. The half time of crystallization is plotted against the ferrite concentration at various cooling rate; open symbol for PA6$_S$-46 and PA6$_S$-60; solid symbol for samples with rough ferrite inside.

tallinity degree (X_t) is calculated at difference temperature T, and the plots of X_t against T are displayed in Fig. 6.

According to Eq. (2) the horizontal T-axis in master graphic of Fig. 6 can be transformed into the crystallization time t-axis as exhibited in lower inset of Fig. 6. It is seen that all of these curves have similar sigmoidal shape, and the curvature of the upper parts of the plot is observed to be level off due to the spherulites impingement [48]. We obtain the half time of crystallization $t_{1/2}$ at X_t = 0.5–50% to eliminate the induction period, as plotted against the ferrite concentration in Fig. 7. It is displayed that $t_{1/2}$ values increased with the increase of ferrite concentration at a given cooling rate, indicating that increased surrounding chains could be slowed and hindered. The interface-induced heterogeneous nucleation, however, decreases the crystallization time by neutralizing the hindering and slowing effect, as compared with the crystallization time of PA6-46 and PA6$_S$-46 depicted in Fig. 7.

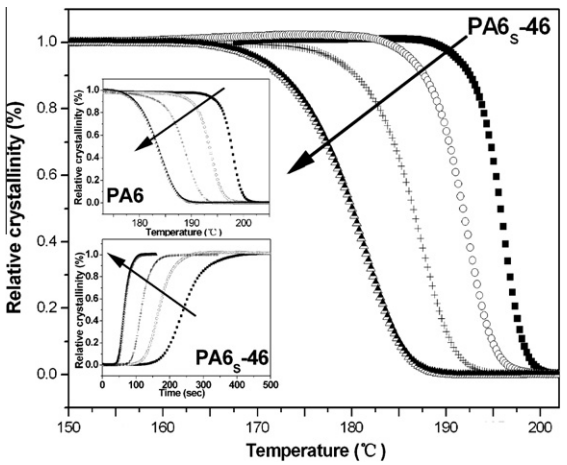

Fig. 6. Relative crystallinity versus temperature for PA6$_S$-46 and PA6 (upper inset); relative crystallinity versus time for PA6$_S$-46 (lower inset). The black arrows from tail to tip indicate the cooling rate of 2.5, 5, 10, 20 °C/min, respectively.

The Avrami equation [49,50] can be applied to describe the isothermal crystallization behavior. Under non-isothermal crystallization, the Avrami equation could still partly explain the primary stage of crystallization, as follows:

$$1 - X_t(T) = \exp(-Z_t t^n), \tag{3}$$

$$\log[-\ln(1 - X_t(T))] = n \log t + \log Z_t, \tag{4}$$

where $X_t(T)$ is the relative degree of crystallinity at time t. Both the parameter Z_t and the Avrami exponent n are diagnostic of the crystallization mechanism. For the non-isothermal crystallization process, the Z_t estimated from Eq. (4) should be inadequate because of the influence of the cooling rate. Jeziorny [51] considered that the parameter Z_t should be corrected as:

$$\log Z_c = \frac{\log Z_t}{a} \tag{5}$$

the values of the Avrami exponent n and the rate parameter Z_t can be obtained from the slope and intercept of the plot of $\log[-\ln(1 - X_t(T)]$ versus $\log t$, as shown in Table 2. The listed data of PA6 is similar with result of Refs. [37,52–55] but higher than that of Refs. [56,57]. It is seen that the n values of pure PA6 vary from 6.2 to 7.6, while these of composites range from 6.5 to 12.9 which means the addition of highly filled particles influences the mechanism of nucleation and the growth of PA6 crystalline. Note that only the n values of pure PA6 which is prepared by extrusion are higher than 4 and vary slightly with molecular weight [58], we believe that these high n values is a reflection of memory effects associated with the processing of polyamide [53]. The linear fits for the plots of $\log[-\ln(1 - X_t(T)]$ versus $\log t$ are typical displayed in Fig. 8. It can be seen that the plots consist of two or three regions, indicating that the Avrami analysis does not well describe non-isothermal crystallization of PA6 and PBMs. It is well known that the parameter of Avrami exponent n relates to the growing mechanism and geometry of crystallization and

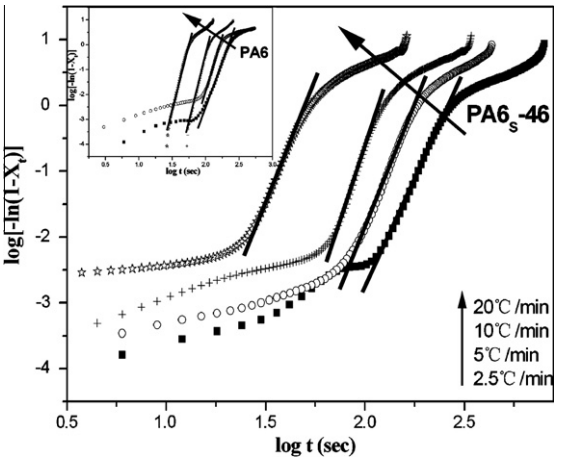

Fig. 8. Plots of $\log(-\ln(1-X_t))$ as a function of $\log t$ for PA6$_S$-46 and PA6 (inset) upon non-isothermal crystallization.

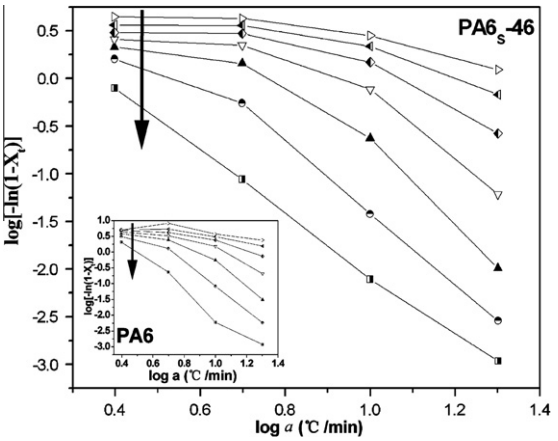

Fig. 9. Ozawa plots of $\log[-\ln(1-X_t)]$ against $\log a$ for PA$_S$-46 and PA6 (inset). The temperatures from top to bottom are 177, 180, 183, 186, 189, 192 and 195 °C, respectively.

the parameter Z_c is determined by the growth rate under the non-isothermal crystallization condition. For all samples, the n values are more than 4 and increase with the growth of cooling rates, indicating that the highly filled ferrites extremely complicate the nucleation mechanisms presumably due to the severely distortion and damage of polymer matrix. Furthermore, the n value of PA6-46 reaching 12.9 at a cooling rate of 20 °C/min is a little higher than that of PA6$_S$-46, suggesting a more complex nucleation mechanism. As imagined, the highly filled ferrites fracture polymer continuous matrix and couple a severely internal stress. Whereas the modified ferrites have chemical affinity to absorb the chain segments and to partially release the internal stress. The nucleation mechanism of PA6 in PA6$_S$-46 sample, hence, is less complicated than that in PA6-46 and obtains a low value of n.

Considering the effect of cooling rate on the non-isothermal crystallization, Ozawa [59] extended the Avrami theory from isothermal crystallization to the non-isothermal case, and modified the Avrami equation as followed:

$$1 - X_t(T) = \exp\left[-\frac{K(T)}{|a|^m}\right], \tag{6}$$

$$\log[-\ln(1 - X_t(T))] = \log K(T) - m\log a, \tag{7}$$

where $K(T)$ is a cooling function depending on the crystallization rate, and m is the Ozawa exponent depending on the dimension of crystal growth. In general, if the Ozawa equation could be accurately accord with the crystallization behavior of polymer, then the plot of $\log[-\ln(1-X_t(t))]$ versus $\log a$ will obtain a precisely straight line. And thus the Ozawa exponent m and $K(T)$ value can be also precisely obtained. Typical Ozawa plots for PA6 and PA6$_S$-46 is displayed in Fig. 9. The crystallization behaviors of PA6 and PBMs are not fitted well with the Ozawa equation because of the curvatures in the plots. Under non-isothermal crystallization, the crystallization rate is no longer a constant but a function of both time and cooling rate [40]. However, these differences do not be taken into account in the Ozawa model. The other ignored factor in the Ozawa model is the temperature dependence of folded chain length of the polymer chain. More detailed interpretation for the deviation of Ozawa model was depicted elsewhere [23,36,37,51].

As mentioned above, both the Avrami and the Ozawa models cannot accurately describe the non-isothermal crystallization kinetic of the PA6 and PBMs. To deeply investigate the non-isothermal crystallization kinetic, Mo et al. [60,61] proposed a combined Avrami and Ozawa equation to describe the non-isothermal crystallization kinetics of polymers, as follows:

$$\log Z_t + n\log t = \log K(T) - m\log a, \tag{8}$$

$$\log a = \log F(T) - b\log t, \tag{9}$$

where the parameters of $F(T)$ and b are equal to $[K(T)/Z_t]^{1/m}$ and n/m, respectively. The Mo equation correlates the cooling rate and the crystallization time under non-isothermal crystallization condition, and could be defined by a certain degree of crystallinity. $F(T)$ refers to the value of cooling rate, chosen at unit crystallization time when the system amounts to a certain degree of crystallinity [48]. Increasing the crystallization rate could reduce the value of $F(T)$. The $-b$ and $\log F(T)$ values are obtained by the slope and intercept of Mo plot of $\log a$ against $\log t$, as tabulated in Table 3. Typical Mo plots of PA6$_S$-46 and PA6 reflect a good linear relationship, indicating that this modal is more effective in describing the non-isothermal crystallization kinetics of PA6 and PBMs (Fig. 10).

Recalling the anomalous crystallinity (see Table 1) and $t_{1/2}$ (see Fig. 7 with cooling rate of 20 °C/min) of PA6-5 compared with that of PA6, we reveal that the addition of a small quantity of ferrites into PA6 matrix promote the mobility of chain segments because some extra spaces introduced on the interfacial layer (see Fig. 2(b)), and hence increase the crystallization rate and crystallinity. This process is independence of cooling rate in the observed range. However, in the relatively low temperature regime, it is possible to arrange the chain segments into crystal lattice only at a low cooling rate (see PA6-5 with cooling rate of 2.5, 5 °C/min in Fig. 7), because a fast cool-

Table 3
Non-isothermal crystallization kinetic parameters based on the Mo method.

X_t (%)	20	40	60	80
PA6				
$F(T)$	1.36	1.42	1.48	1.55
b	1.92	1.88	1.84	1.80
PA6-5				
$F(T)$	1.38	1.45	1.52	1.61
b	2.00	1.96	1.92	1.88
PA6-20				
$F(T)$	1.40	1.49	1.53	1.66
b	2.09	2.08	2.01	1.95
PA6-46				
$F(T)$	1.51	1.58	1.65	1.71
b	1.84	1.79	1.79	1.72
$PA6_S$-46				
$F(T)$	1.30	1.39	1.46	1.53
b	1.58	1.61	1.60	1.52
$PA6_S$-60				
$F(T)$	1.38	1.48	1.57	1.68
b	1.84	1.84	1.83	1.77

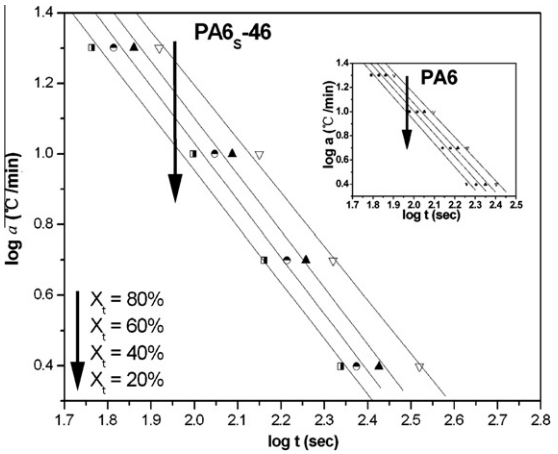

Fig. 10. Plots of $\log a$ against $\log t$ from the Mo method at different relative degrees of crystallinity for $PA6_S$-46 and PA6 (inset).

ing is easy to access a temperature under which the polymer chains can be totally frozen and then, at this time, the contribution of extra space on the mobility of chain segments is negligible. If we extend this scenario to all the samples of PA6 bonded rough ferrites, it is found that the PBMs obtain higher crystallization rates in the primary stage (see Z_c in Table 2) at the low cooling rate than PA6. The extra-space enhanced mobility of segments is responsible for this increasing. However, the global crystallization rate of these (see $F(T)$ in Table 3) are always lower. Thus, the hindering effect is always dominant upon the whole crystallization process. The anomalous crystallinity of PA6-5 is merely because the concentration of ferrites is low and the hindering effect is weak.

3.4. Activation energy for non-isothermal crystallization

To obtain an insight into the relation between non-isothermal crystallization and composite intrinsic characteristic, the activation energy upon non-isothermal crystallization condition could be estimated as follows [62]:

$$\frac{d[\ln(a/T_p^2)]}{d(1/T_p)} = -\frac{\Delta E_a}{R}, \tag{10}$$

where R is the universal gas constant, ΔE_a is the crystallization activation energy. The crystallization activation energy could be obtained from the slope of the plot of $\ln(a/T_p^2)$ versus $1/T_p$, according to Eq. (10), as shown in Fig. 11. The linear concentration dependence of ΔE_a is observed over a concentration scale less than 20 vol % and starts a deviation with the concentration up to 46 vol % for the rough ferrites inside sample. Note that, the ferrite particle surface area is also as a linear function of particle quantity. As the minimal particle length is an order of magnitude larger than Kuhn length of PA6 chain, and therefore, we envisage that the ferrites with various size lengths are equal to the influence of the motion of chain segments. Lots of researches have already confirmed that the size distribution did not affect the crystallization process [11,23,25,63]. The other presumption is the thickness of interfacial space for particles with different size, is equal. Thus, we believe that the concentration of particles was as a reverse function of ΔE_a. It is clear that the deviation of PA6-46 in Fig. 11 is attributed to the particle agglomeration. The plot of ΔE_a against ferrite concentration, therefore, also can evaluate the dispersion performance of hydrophilic fillers within hydrophobic polymer.

The ΔE_a increases with the increase of modified ferrites, indicating that the enhanced interaction requires more energy to arrange the segments upon crystallization. Since only two data is obtained in our measurement, we do not precisely confirm the relation between enhanced interfacial area and ΔE_a, which also could be severely impacted by agglomeration or incomplete modification. But it still demonstrates a strong interfacial strength of particle–polymer layer and is grounds of argument to support the experimental observations and discussions above.

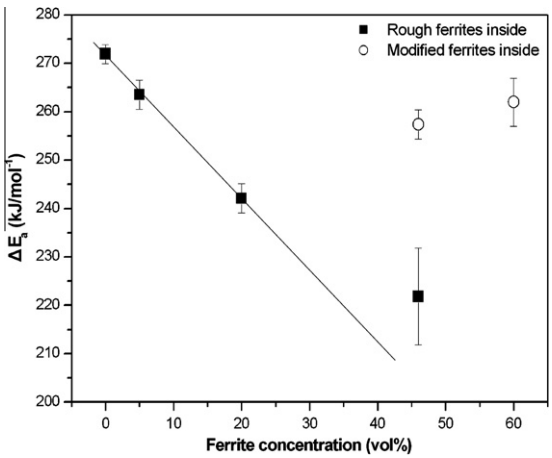

Fig. 11. Crystallization activation energies ΔE_a of the PA6 as a function of ferrite concentration. The error bars indicate the average of total 10 measurements preformed by different samples.

4. Conclusion

Polyamide 6 bonded ferrites was prepared by melt extrusion. The highly filled rough ferrites within PA6 gave rise to a distortion and damage of PA6. The study on non-isothermal crystallization revealed that the highly filled ferrite particles with irrespective of surface nature could severely hinder the motion of surrounding chain segments. However, a blurry interface between silane modified ferrites and PA6 matrix was observed, implying a good interfacial strength. Increasing this type of enhanced interfacial area between polymer–particles could promote the heterogeneous nucleation. A good interaction however, could also slow the motion of surrounding chain segments of particle. PA6-5 obtain a high crystallinity on the basis of a different mechanism: the addition of a small quantity of ferrites into PA6 matrix made it possible to arrange the chain segments into crystal lattice even at a relatively low temperature because some extra space introduced by interfacial layer, promoted the mobility of chain segments. The crystallization kinetic of PA6 bonded rough ferrites reveal the effect of extra space on crystallization process always exists and is distinct only if both the cooling rate and concentration of hydrophilic ferrites are low. In a word, the slowing effect, heterogeneous nucleation, hindering effect and extra space within polymer matrix act concurrently upon crystallization process. The Mo method was found to be effective in describing the non-isothermal crystallization of polyamide 6 boned ferrites. The plot of ΔE_a against ferrite concentration also could be utilized to evaluate a dispersion performance of hydrophilic fillers within hydrophobic polymer.

Acknowledgements

The authors express their gratefulness for the financial support from National Natural Science Foundation of China (Grant No. 50673047) and Grand Science and Technology Special of Shandong province of China (Grant No. 2006GG1103085). W.D. thanks the Max Planck Society (Germany) for a financial support.

References

[1] Otaigbe J, Kim H, Xiao J. Effect of coupling agent and filler particle size on melt rheology of polymer-bonded Nd–Fe–B magnets. Polym Compos 1999;20(5):697–704.
[2] Xiao J, Otaigbe J. Polymer-bonded magnets. III. Effect of surface modification and particle size on the improved oxidation and corrosion resistance of magnetic rare earth fillers. J Alloy Compd 2000;309(1–2):100–6.
[3] Zhang XH, Xiong WH. Effect of bonding process on the properties of isotropic epoxy resin-bonded Nd–Fe–B magnets. Rare Met 2009;28(3):248–52.
[4] Bai SX, Zhang H, Lv L, et al. Progress of research on bonded Nd–Fe–B magnets. J Iron Steel Res Int 2006;13:489–93.
[5] Romero JJ, Cuadrado R, Pina E, et al. Anisotropic polymer bonded hard-magnetic films for microelectromechanical system applications. J Appl Phys 2006;99(8):303.
[6] Yudin VE, Otaigbe JU, Bui TX, Svetlichnyi VM. Structure and properties of polyimide-bonded magnets processed from prepolymers based on diacetyl derivatives of aromatic diamines and dianhydrides. J Appl Polym Sci 2006;100(1):478–85.
[7] Hemrick J, Lara-Curzio E, Liu K. Mechanical properties of thermally cycled nylon bonded Nd–Fe–B permanent magnets. J Mater Sci 2004;39(21):6509–22.
[8] Makled MH, Matsui T, Tsuda H, Mabuchi H, El-Mansy MK, Morii K. Magnetic and dynamic mechanical properties of barium ferrite–natural rubber composites. J Mater Process Technol 2005;160(2):229–33.
[9] Rada M, Kardelky S, Mazilu I, et al. Corrosion behavior of polymer-bonded NdFeB-based nanocrystalline magnets. IEEE Trans Magn 2004;40(4):2864–6.
[10] Yudin VE, Otaigbe JU, Bui TX, Svetlichnyi VM. Polyimide bonded magnets: processing and properties. J Appl Polym Sci 2003;88(14):3151–8.
[11] Guschl PC, Kim HS, Otaigbe JU. Effects of a Nd–Fe–B magnetic filler on the crystallization of poly(phenylene sulfide). J Appl Polym Sci 2002;83(5):1091–102.
[12] Matutes-Aquino J, Rios-Jara D, Ayala-Valenzuela O, Gallardo PS, De Valle LFR, Fernandez OSR. Composition dependence of the magnetic properties of banded magnets of strontium hexaferrite-polyvinyl chloride. Polym Compos 2000;21(5):734–8.
[13] Xiao J, Otaigbe JU, Jiles DC. Modeling of magnetic properties of polymer bonded Nd–Fe–B magnets with surface modifications. J Magn Magn Mater 2000;218(1):60–6.
[14] Xiao J, Otaigbe JU. Polymer bonded magnets. II. Effect of liquid crystal polymer and surface modification on magneto-mechanical properties. Polym Compos 2000;21(2):332–42.
[15] Jun X, Otaigbe JU. Polymer-bonded magnets. I. Analytic thermogravimetry to determine the effect of surface modification on dispersion of Nd–Fe–B fillers. J Mater Res 1999;14(7):2893–6.
[16] Otaigbe JU, Kim HS, Xiao J. Effect of coupling agent and filler particle size on melt rheology of polymer-bonded Nd–Fe–B magnets. Polym Compos 1999;20(5):697–704.
[17] Otaigbe JU, Xiao J, Kim H, Constantinides S. Influence of filler surface treatments on processability and properties of polymer-bonded Nd–Fe–B magnets. J Mater Sci Lett 1999;18(4):329–32.
[18] Xiao J, Otaigbe JU. Polymer-bonded magnets. Part I: Analytic thermogravimetry to determine the effect of surface modification on dispersion of Nd–Fe–B fillers. J Mater Res 1999;14(7):2893–6.
[19] Liu AZ, Rahman IZ, Rahman MA, Petty ER. Fabrication and measurements on polymer bonded NdFeB magnets. J Mater Process Technol 1996;56(1–4):571–80.
[20] Wu H, Zheng R, Xie Z. Enhancing mechanical properties and magnetic performance of plastics magnet via mixing under vibration force field. J Mater Process Technol 2009;209(2):1048–52.
[21] Kim J, Park H, Kim S. Unique nucleation of multi-walled carbon nanotube and poly(ethylene 2,6-naphthalate) nanocomposites during non-isothermal crystallization. Polymer 2006;47(4):1379–89.
[22] Khalil R, Chryss A, Jollands M, Bhattacharya S. Effect of coupling agents on the crystallinity and viscoelastic properties of composites of rice hull ash-filled polypropylene. J Mater Sci 2007;42(24):10219–27.
[23] Xie Y, Yu D, Kong J, Fan X, Qiao W. Study on morphology, crystallization behaviors of highly filled maleated polyethylene-layered silicate nanocomposites. J Appl Polym Sci 2006;100(5):4004–401.
[24] Zerda A, Caskey T, Lesser A. Highly concentrated, intercalated silicate nanocomposites: synthesis and characterization. Macromolecules 2003;36(5):1603–8.
[25] Ren Z, Shanks R, Rook T. Crystallization and melting of highly filled polypropylene composites prepared with surface-treated fillers. J Appl Polym Sci 2001;79(11):1942–8.
[26] Broekaert C, Peeterbroeck S, Benali S, et al. Chlorinated polyethylene/layered silicate nanocomposites: poly(epsilon-caprolactone)-based "masterbatch" approach. Eur Poly J 2007;43(10):4160–8.
[27] Ramirez F, Carlsson L. Modified single fiber fragmentation test procedure to study water degradation of the fiber/matrix interface toughness of glass/vinylester. J Mater Sci 2009;44(12):3035–42.
[28] Hsiang H, Tsai J. Titanate coupling agent effects on nonaqueous Co 2 Z ferrite suspensions dispersion. J Mater Sci 2006;41(19):6339–46.
[29] Shelley JS, Mather PT, DeVries KL. Reinforcement and environmental degradation of nylon-6/clay nanocomposites. Polymer 2001;42(13):5849–58.
[30] Shi J, Wang Y, Gao Y, Bai HW. Effects of coupling agents on the impact fracture behaviors of T-ZnOw/PA6 composites. Compos Sci Technol 2008;68(6):1338–47.
[31] Garcia D, Starkweather HW. Hydrogen-bonding in nylon-66 and model compounds. J Polym Sci B Polym Phys 1985;23(3):537–55.
[32] Wan T, Clifford MJ, Gao F, Bailey AS, Gregory DH, Somsunan R. Strain amplitude response and the microstructure of PA/clay nanocomposites. Polymer 2005;46(17):6429–36.

[33] Skrovanek DJ, Painter PC, Coleman MM. Hydrogen-bonding in polymers. 2. Infrared temperature studies of nylon-11. Macromolecules 1986;19(3):699–705.
[34] Roberts MF, Jenekhe SA. Site-specific reversible scission of hydrogen-bonds in polymers – an investigation of polyamides and their lewis acid–base complexes by infrared-spectroscopy. Macromolecules 1991;24(11):3142–6.
[35] Ma Y, Hu G, Ren X, Wang B. Non-isothermal crystallization kinetics and melting behaviors of nylon 11/tetrapod-shaped ZnO whisker (T-ZnOw) composites. Mater Sci Eng A 2007;460:611–8.
[36] Kuo M, Huang J, Chen M. Non-isothermal crystallization kinetic behavior of alumina nanoparticle filled poly(ether ether ketone). Mater Chem Phys 2006;99(2–3):258–68.
[37] Li J, Fang Z, Tong L, Gu A, Liu F. Effect of multi-walled carbon nanotubes on non-isothermal crystallization kinetics of polyamide 6. Eur Poly J 2006;42(12):3230–5.
[38] Wei C, Srivastava D, Cho K. Thermal expansion and diffusion coefficients of carbon nanotube–polymer composites. Nano Lett 2002;2(6):647–50.
[39] Cheng S, Wunderlich B. Glass transition and melting behavior of poly(ethylene 2,6-naphthalenedicarboxylate). Macromolecules 1988;21(3):789–97.
[40] Kim S, Ahn S, Hirai T. Crystallization kinetics and nucleation activity of silica nanoparticle-filled poly(ethylene 2,6-naphthalate). Polymer 2003;44(19):5625–34.
[41] Li L, Li C, Ni C, Rong L, Hsiao B. Structure and crystallization behavior of Nylon 66/multi-walled carbon nanotube nanocomposites at low carbon nanotube contents. Polymer 2007;48(12):3452–60.
[42] Zhao C, Zhang P, Lu S, He J, Wang X. Study on the non-isothermal crystallization behaviors of PA6/silica nanocomposites prepared by the sol–gel process. J Mater Sci 2007;42(21):9083–91.
[43] Wang C, Huang C, Chen Y, Hwang G, Tsai S. Carbon nanocapsules-reinforced syndiotactic polystyrene nanocomposites: crystallization and morphological features. Polymer 2008;49(25):5564–74.
[44] Kim K, Park N, Ryu K, Chang S. Characterization of poly(vinylidenefluoride-co-hexafluoropropylene)-based polymer electrolyte filled with TiO_2 nanoparticles. Polymer 2002;43(14): 3951–7.
[45] Hinrichsen G, Lux F. Crystallization kinetics of highly filled glass fibre/polyamide 6 composites. Polym Bull 1990;24(1):79–86.
[46] Chae DW, Lee KH, Kim YC. Rheological properties of ferrite nanocomposites based on nylon-66. J Polym Sci B Polym Phys 2006;44(2):371–7.
[47] Illers K. Polymorphie, kristallinit t und schmelzw rme von poly(ε-caprolactam), 2. Teil 1: cf. 3. Kalorimetrische untersuchungen. Die Makromol Chem 1978;179(2):497–507.
[48] Run M, Wang Y, Yao C, Gao J. Non-isothermal crystallization kinetics of poly(trimethylene terephthalate)/poly(ethylene 2,6-naphthalate) blends. Thermochim Acta 2006;447(1):13–21.
[49] Weng W, Chen G, Wu D. Crystallization kinetics and melting behaviors of nylon 6/foliated graphite nanocomposites. Polymer 2003;44(26):8119–32.
[50] Avrami M. Kinetics of phase change. I. General theory. J Chem Phys 1939;7:1103.
[51] Jeziorny A. Parameters characterizing the kinetics of the non-isothermal crystallization of poly(ethylene terephthalate) determined by DSC. Polymer 1978;19(10):1142–4.
[52] Li LY, Li CY, Ni CY, Rong LX, Hsiao B. Structure and crystallization behavior of Nylon 66/multi-walled carbon nanotube nanocomposites at low carbon nanotube contents. Polymer 2007;48(12):3452–60.
[53] Fornes T, Paul D. Crystallization behavior of nylon 6 nanocomposites. Polymer 2003;44(14):3945–61.
[54] Privalko V, Kawai T, Lipalov Y. Crystallization of filled nylon 6. III. Non-isothermal crystallization. Colloid Polym Sci 1979;257(10):1042–8.
[55] Chuah K, Gan S, Chee K. Determination of Avrami exponent by differential scanning calorimetry for non-isothermal crystallization of polymers. Polymer (Guildford) 1999;40(1):253–9.
[56] Weng WG, Chen GH, Wu DJ. Crystallization kinetics and melting behaviors of nylon 6/foliated graphite nanocomposites. Polymer 2003;44(26):8119–32.
[57] Monteiro-Riviere N, Nemanich R, Inman A, Wang Y, Riviere J. Multi-walled carbon nanotube interactions with human epidermal keratinocytes. Toxicol Lett 2005;155(3):377–84.
[58] Khanna YP, Reimschuessel AC, Banerjie A, Altman C. Memory effects in polymers. 2. Processing history vs crystallization rate of nylon-6 observation of phenomenon and product behavior. Polym Eng Sci 1988;28(24):1600–6.
[59] Ozawa T. Kinetics of non-isothermal crystallization. Polymer 1971;12(3):150–8.
[60] Liu T, Mo Z, Wang S, Zhang H. Nonisothermal melt and cold crystallization kinetics of poly(aryl ether ether ketone ketone). Polym Eng Sci 1997;37(3):568–75.
[61] Liu M, Zhao Q, Wang Y, Zhang C, Mo Z, Cao S. Melting behaviors, isothermal and non-isothermal crystallization kinetics of nylon 1212. Polymer 2003;44(8):2537–45.
[62] Kissinger H. Variation of peak temperature with heating rate in differential thermal analysis. J Res Natl Bureau Stand 1956;57(4):217–21.
[63] Hauser R, King J, Pagel R, Keith J. Effects of carbon fillers on the thermal conductivity of highly filled liquid-crystal polymer based resins. J Appl Polym Sci 2008;109(4):2145–55.